Proceedings of the ASME 2021 16th International Manufacturing Science and Engineering Conference
MSEC2021
June 21-25, 2021, Virtual, Online

MSEC2021-63687

PRECISION EVALUATION OF NEXUS, A CUSTOM MULTI-ROBOT SYSTEM FOR MICROSYSTEM INTEGRATION

Danming Wei[1], Alireza Tofangchi, Andriy Sherehiy, Mohammad Hossein Saadatzi, Moath Alqatamin, Keng Hsu, Dan O. Popa
Louisville Automation and Robotic Research Institute (LARRI),
University of Louisville, Louisville, Kentucky, USA

ABSTRACT

Industrial robots, as mature and high-efficient equipment, have been applied to various fields, such as vehicle manufacturing, product packaging, painting, welding, and medical surgery. Most industrial robots are only operating in their own workspace, in other words, they are floor-mounted at the fixed locations. Just some industrial robots are wall-mounted on one linear rail based on the applications. Sometimes, industrial robots are ceiling-mounted on an X-Y gantry to perform upside-down manipulation tasks. The main objective of this paper is to describe the NeXus, a custom robotic system that has been designed for precision microsystem integration tasks with such a gantry. The system tasks include assembly, bonding, and 3D printing of sensor arrays, solar cells, and microrobotic prototypes. The NeXus consists of a custom designed frame, providing structural rigidity, a large overhead X-Y gantry carrying a 6 degrees of freedom industrial robot, and several other precision positioners and processes. We focus here on the design and precision evaluation of the overhead ceiling-mounted industrial robot of NeXus and its supporting frame. We first simulated the behavior of the frame using Finite Element Analysis (FEA), then experimentally evaluated the pose repeatability of the robot end-effector using three different types of sensors. Results verify that the performance objectives of the design are achieved.

Keywords: industrial robot, custom frame, natural frequency, repeatability,

1. INTRODUCTION

In recent years, industrial robots have been increasingly used in 3D printing and microsystem integration applications. Bhatt [1] developed a robotic cell with two ABB industrial robotic arms, ABB IRB120 and ABB IRB2600, for multi-resolution additive manufacturing with 3D printing techniques. Yoon [2] integrated a three-nozzle extrusion system with Yaskawa Motoman GP12 industrial robot to realize conformal multi-resolution 3D printing. Otherwise, it is significantly necessary to evaluate industrial robots before using the robot to execute tasks in the research. Brethé [3] evaluated the repeatability of a Kuka IR364 industrial robot using the stochastic ellipsoid approach method. Morozov [4] assessed the accuracy of a Kuka KR5 arc HW robotic arm for the enhancement of automated non-destructive testing. Baker [5] evaluated Universal Robots UR10 robotic arm for the development of repeatability procedures. Kuric [6] dealed with the measurement of pose repeatability of Fanuc LR Mate 200iC industrial robot. The industrial robot manufacturers mentioned above are from different countries all over the world. Therefore, they all use standards regulated by the International Organization for Standardization (ISO) to evaluate their industrial robots' performance. ISO9283:1998 standard [7] is adopted to determine pose repeatability and many other performance criteria of manipulating industrial robots.

The NeXus is a custom designed multi-robot system targeting microsystem integration using several assembly, 3D printing, and bonding processes. A prototype of the human-machine interface for the microassembly station of the NeXus has been designed and evaluated [8, 9]. Also, the 3D printing technique has been investigated for the NeXus, including a dual-head fused deposition modeling (FDM) 3D printing technique [10], and integrating Aerosol Jetting and dispenser Auger valve additive manufacturing subsystems [11]. The bonding process

[1] Danming Wei: danming.wei@louisville.edu

has been developed using ultrasonic vibration techniques to print metal wire on a polymer surface [12, 13]. As a part of the system, we designed and built a 3960mm x 3530mm x 2215mm (L x W x H) modular frame, on which a large 2D gantry is carrying a 6 degrees of freedom (DOF) industrial robotic arm. This paper presents our design, along with simulation and analysis, as well as the evaluation of end-effector positioning precision of the robotic arm using the ISO9283:1998 standard.

The paper is organized in the following orders: in Section 2, we briefly describe the NeXus robotic system and focus on the design of the custom frame integrated with X-Y gantry and industrial robotic arm; and also presents the different designs and simulation results of the custom frame; in Section 3, we study static evaluation of the natural frequency and pose accuracy and repeatability performance of the end-effector of robotic arm; in Section 4, we discuss the results of the experiments of pose accuracy and repeatability via different sensors; finally, in Section 5, we conclude the paper and discuss the future works.

2. DESIGN OF NEXUS

NeXus is a novel custom robotic system for multiscale additive manufacturing with integrated 3D printing techniques and robotic assembly. The NeXus has several subsystems, such as a microassembly station, an aerosol jetting print station, an intense pulsed light (IPL) photonic sintering station, a fiber weaving station, and a 3D printing station. Material handling and positioning inside NeXus are achieved with the help of two industrial robotic arms with 6-DOF and 4-DOF, respectively. The 6-DOF overhead mounted arm is responsible for substrate and parts tray movement among several additive manufacturing processes. The 4-DOF robot is responsible for pick and place of electronic components for Printed Circuit Board applications and positioning tools in conjunction with textile weaving. Figure 1 shows the overall design of the NeXus and the location of subsystems.

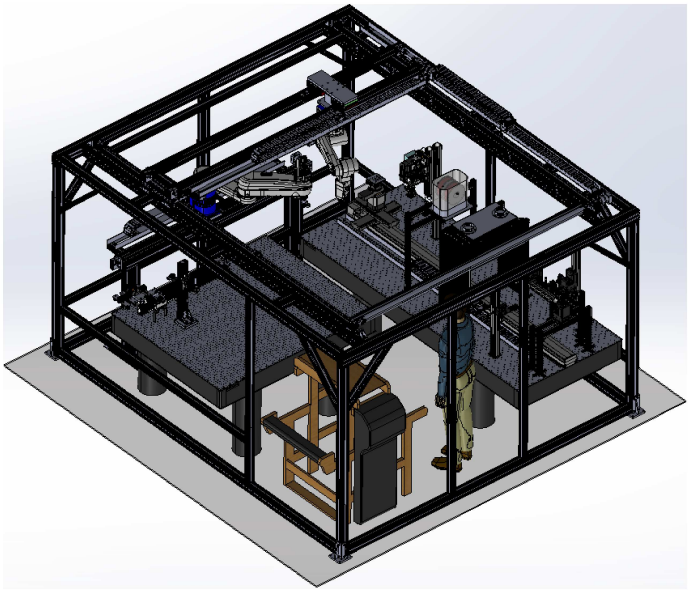

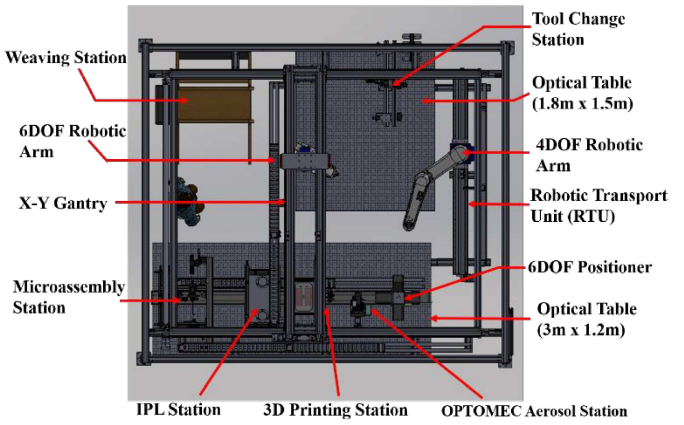

FIGURE 1: DESIGN OF THE NEXUS INDICATING THE INDUSTRIAL ROBOTS AND THE SYSTEM FRAME

For different applications, several modular quick-change tools equipped with end-effectors are available for pick up by industrial robots. These tools include microgrippers for micromanipulation, an ultrasonic head for bonding of metals and polymers, and vacuum nozzles or suction cups for assembling the specific components.

The industrial robotic arms, as the main assistant tools, will be used to transfer the various components among the different subsystems. To maximize the workspace of the 6-DOF industrial robot DENSO VS-6577B (DENSO Corporation, CA, USA), we proposed a solution where the robotic arm was ceiling mounted on a large X-Y gantry (Macron Dynamics, Inc., PA, USA) with a 2800mm x 2250mm (X x Y) travel range. The gantry is fixed on a custom frame (Monarch Automation, Inc., OH, USA) with dimensions 3960mm x 3530mm x 2215mm (L x W x H), as shown in Figure 2.

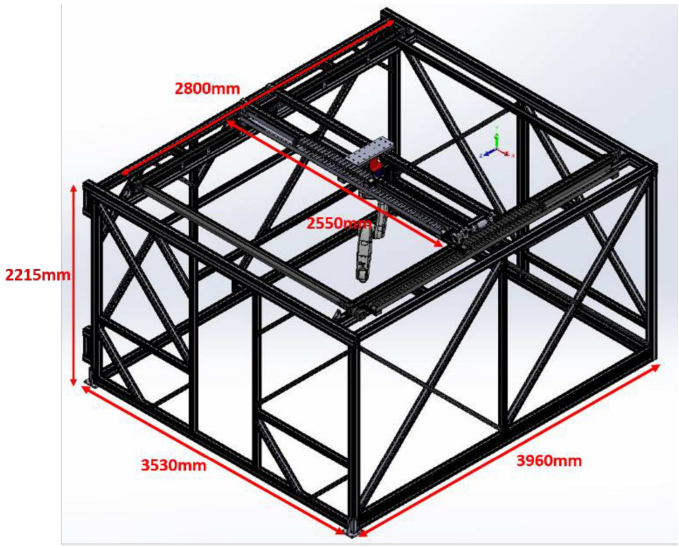

FIGURE 2: THE ISOMETRIC VIEW OF THE CUSTOM FRAME WITH MOUNTED X-Y GANTRY AND AN INDUSTRIAL ROBOTIC ARM

The frame is proposed to carry more than 250kg payload, which includes the X-Y gantry and robotic arm. The ceiling-mounted industrial robotic arm can operate with accuracy and repeatability under 50µm existing the uncertainties of custom frame, X-Y gantry, and corresponding adapters. The workspace of the robotic arm along with the X-Y gantry can reach approximately 3.5m x 3.5m x 1m.

2.1 DESIGN OF THE CUSTOM FRAME

This section mainly focuses on structural analysis of the frame design to justify the modifications needed to improve its stability. We performed simulations that determine natural frequencies and deflections of the frame structure.

The custom frame was designed to support the X-Y gantry with a ceiling-mounted 6-DOF robotic arm. The stiffness and stability of the frame will consequently influence the motion performance of the robotic arm, which is especially critical for high-precision assembly applications.

The entire frame assembly, which can be viewed as a multi-member mechanical structure, exhibits various natural frequencies with corresponding modal shapes (eigenvalues). Due to the complexity of the structure, we used a Finite Element Analysis (FEA) simulation software COMSOL® to estimate the modal frequencies and mode shapes as well as deformation under a static load. The amplitude of each vibrational mode depends on the external moving objects attached to the frame, such as the gantry's body and the robotic arm.

In the frame design process, we used the notion of frequency (f) in a structure as a function of mass (M) and mechanical stiffness (K) which is conceptually described in Equation 1:

$$f \sim \sqrt{K/M} \tag{1}$$

Hence, by increasing the stiffness of the structure, the natural frequency also tends to increase which is favorable. The attachment of additional beams to the structure would increase the bulk stiffness of the frame. The COMSOL® software served to visualize the progressive improvement that emerged in the frame quantitatively and assisted us to optimize the final arrangement of the beams in the frame.

In Figure 3, we proposed an initial modular design of the custom frame, which is dimensionally and structurally sound. However, vibration amplitudes have also been investigated to improve the initial design frame structure. Progressive modifications of the frame have been achieved with simulation analysis of various arrays of the frame design.

In the COMSOL® simulation, the static load was placed on the top of the frame, representing the combined weight of gantry (M_{gantry} =175kg) and robot (M_{robot}=50kg). Here, the robot's mass includes the mass of the robot's body, adapters, and an end-effector. Total static and inertia loads were applied in X, Y, and Z directions. With given maximum acceleration (a) data from the manufacturer in all 3 axes, each of the corresponding force (F) component is calculated from the following Equations:

$$a_x = a_y = 10\,m/s^2, a_z = 5\,m/s^2 \tag{2}$$

$$F_x = M_{robot} \times a_x = 500N \tag{3}$$

$$F_y = M_{robot} \times a_y = 500N \tag{4}$$

$$F_z = M_{robot} \times (a_z + 9.81) + M_{gantry} \times 9.81 = 2456N \tag{5}$$

Firstly, a quasi-static analysis was completed following the five locations of lumped mass on the gantry as shown in Figure 3. Figure 4 depicts the subsequent deformations of beams when the lumps mass located at the center and the corner of the gantry respectively. Otherwise, in the case of the dynamic analysis, Figure 5 displays three mode shapes (two translational and one rotational) and associated eigenfrequencies (EF) of the entire frame for the initial design.

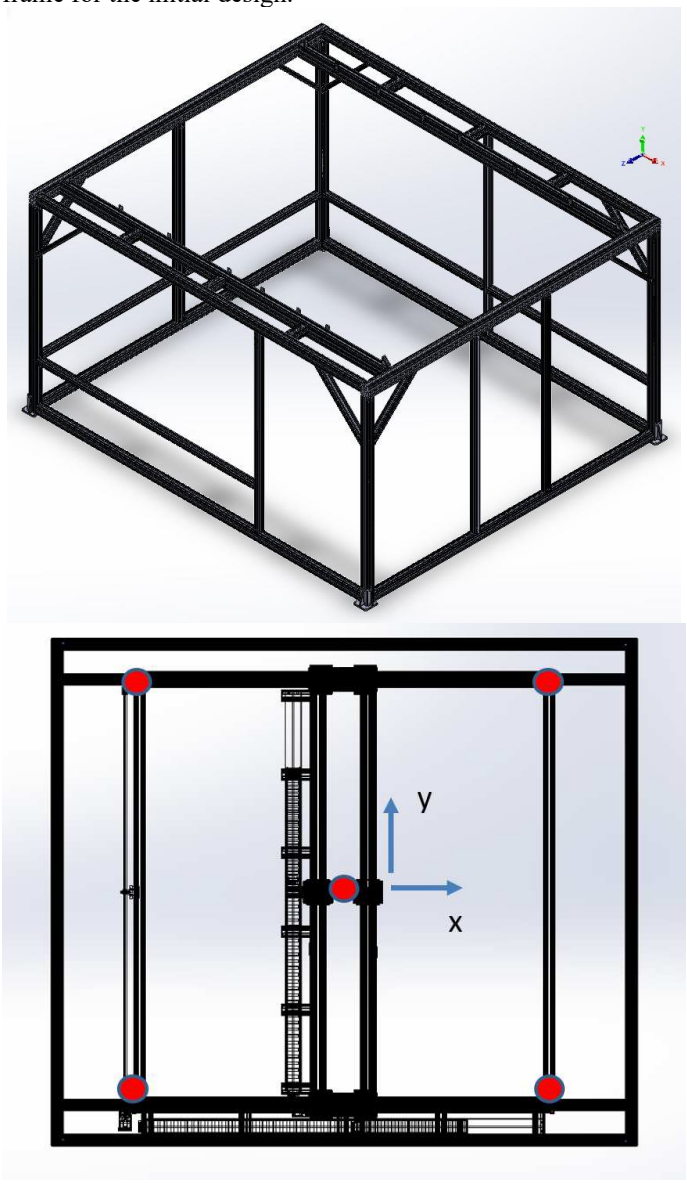

FIGURE 3: TOP: THE INITIAL DESIGN OF THE CUSTOM FRAME; BOTTOM: 5 LOCATIONS OF LUMPED MASS ON THE GANTRY (TOP VIEW)

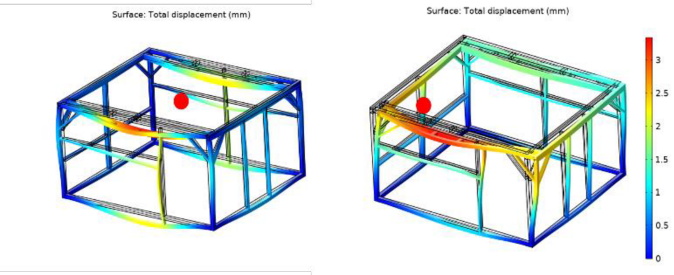

FIGURE 4: THE QUASI-STATIC ANALYSIS FOR THE INITIAL DESIGN OF THE FRAME: THE LOAD AT THE CENTER (LEFT) AND ONE CORNER (RIGHT)

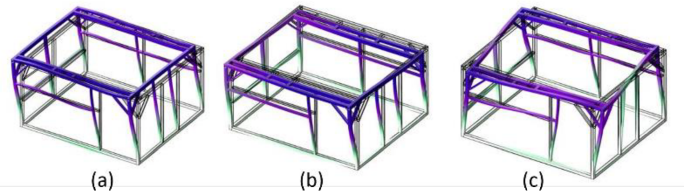

FIGURE 5: INITIAL DESIGN FRAME VIBRATIONAL MODE SHAPES WITH THREE DIFFERENT EIGENFREQUENCIES

For this analysis, the accelerated motions of the robot and the gantry were incorporated to calculate the effective forces acting on the frame, which were also used as inputs to the simulation software. The load sign can vary as the robot and gantry move in various directions. In terms of structural optimization, started with the initial design, we applied several progressive modifications to the frame to improve its stability and mitigate vibrational amplitude during robot translation. The process of the initial and succeeding modified designs can be briefly described as follows, shown in Figure 4-6: in "initial design", the frame was fixed on the ground on its four corners with no additional buttress and interior beams, which suffered from shaking and observable deformation. The "2nd version" with lower beams anchored to the ground at 8 points, showed diminished vibrations on the base beams but not on the entire frame. The "3rd version" with small diagonal beams attached at each corner, showed a significant reduction in frame vibrations in all directions. The "4th version" with reinforced pillar did not serve to be a practical solution spatially, although showed an admissible response. Lastly, in the "final version" longer diagonal beams were used which led to further vibrational mitigations and structural deformation. Thus, in all cases, the revised designs resulted in improvement both in static and dynamic responses (increase eigenfrequencies and reduced maximum deformation), as depicted in Figure 6 and summarized in Table 1. Note that only the 1st mode shape and the maximum deformation for the worst-case scenario have been shown and listed in progressive design versions. Compared with the initial design, the final version of the frame features a significant reduction in the maximum deformation (from 3.5mm to 0.8mm), and a noticeably increased frequency of the lowest eigenfrequency (from 11.1Hz to 19.9Hz).

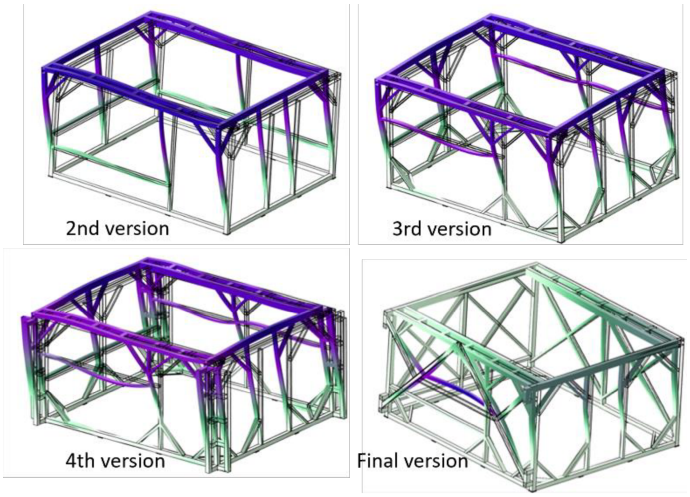

FIGURE 6: FRAME DEFORMATION UNDER THREE DIFFERENT EIGENFREQUENCIES

TABLE 1: EIGENFREQUENCIES AND MAXIMUM DISPLACEMENT OF DIFFERENT VERSION OF FRAME DESIGN

Version of frame design	EF_1 (Hz)	EF_2 (Hz)	EF_3 (Hz)	Max δ (mm)
Initial version	11.1	12.6	14.8	3.5
2nd version	12.7	13.6	15.8	3.0
3rd version	18.3	20.6	22.2	1.2
4th version	23.4	25.4	27.4	0.9
Final version	19.9	23.8	32.6	0.8

δ: displacement in mm

The values of EF_1, EF_2, and EF_3 are the first three eigenfrequencies estimated by FEA corresponding to the natural modes for the "same" loading cases on the frame. Practically, for design purposes, the lowest value of EF for each frame configuration is the matter of interest to avoid severe vibration in the structure. As is evident from Table 1, through each step of progressive modifications of the frame by adding and rearranging the beams, the eigenfrequency also varies. Of particular interest, the lowest eigenfrequency in each design increases from the initial version through the final version by a factor of 2 (1st column in Table 1), which is desirable.

3. EXPERIMENTAL EVALUATION

After completing the assembly of the final version of the frame and mounting the gantry and robotic arm onto the frame, prior to the study of the precision metrics, it is necessary to evaluate the stability of the (frame + gantry + robot) system in a static mode when the gantry and the robotic arm are at rest. The evaluation included measurements of the robotic arm vibrations (noise level) and determination of the natural frequency of the gantry and robotic arm in a static mode. These measurements

were conducted with the help of two Keyence® LK-G5000 (Keyence Corporation, IL, USA) laser displacement sensors as shown in Figure 7. Two sensors were set up to measure the variations of the amplitudes of the natural vibrations along the X-axis and Y-axis. The sampling frequency of the sensor was configurated at 50KHz to collect 2^{19} = 524288 points to determine the natural frequencies of the robotic arm system. Otherwise, the measurements were given in two modes: the robotic arm motor on (brake off) and motor off (brake on). In these ways, it can indicate the influence of the motor status on the natural frequency of the robotic arm.

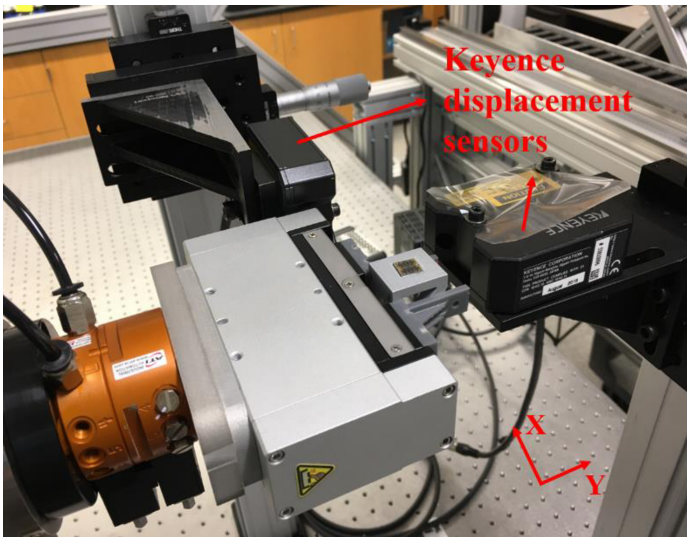

FIGURE 7: TWO LASER DISPLACEMENT SENSORS MEASURE THE NATURAL FREQUENCY OF THE ROBOT ARM

After measuring the natural frequency of the robotic arm in the static mode, we evaluated the robotic arm positioning performance. The 6-DOF industrial robotic arm used in the NeXus has the following specifications based on its manual: maximum payload capacity of 7kg, maximum reach of 850mm, and repeatability of +/- 30µm. However, our custom robotic system containing the X-Y gantry and robot arm has a combined 8 degrees of freedom, and its precision needed to be evaluated with 8-DOF movements. To evaluate the robotic arm, an end-effector, including an ATI Gamma force/torque sensor (ATI Industrial Automation, Inc., NC, USA), an ATI QC-11 tool changer couple, and a HIWIN XEG-32 electrical gripper (HIWIN Corporation, IL, USA) mounted at the end of the robotic arm as shown in Figure 7. The gripper held a 3D cube, onto which we mounted a 1cm x 1cm Silicon die with micron-scale features to serve as the target for visual measurements. To evaluate the pose accuracy and repeatability of the robotic arm, three different measurement sensors are employed: An integrated microscope camera (a combination of Edmund® EO-3112C camera, 7X zoom module motorized lens, and 2.0X lower lens) was calibrated at 70% magnification of the maximum zoom, which results in a resolution of 0.556µm/pixel to monitoring the target in a proper view; two Keyence® LK-G5000 laser displacement sensors with 0.0001mm resolution; and a Mitutoyo 534-390 Digimatic® indicator with 0.001mm resolution.

The first method to evaluate the pose accuracy and repeatability is using the microscope camera. Because the camera only has one degree of freedom, it only acquires 2D information from the image. To measure spatial variables, the microscope camera was set up in horizontal and vertical orientations (shown in Figure 8) to collect X-Y-Z axes data of every single point.

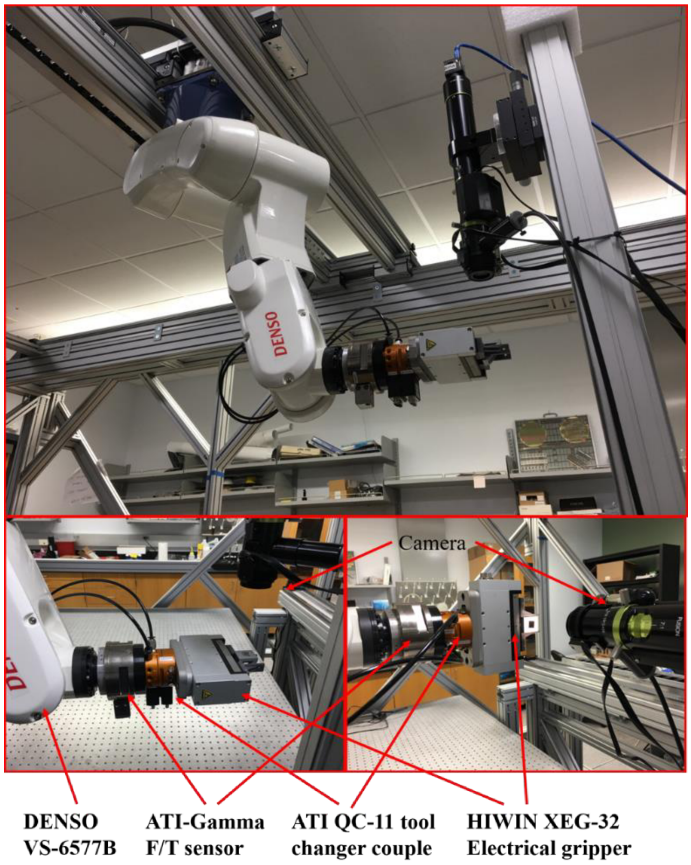

FIGURE 8: HARDWARE SETUP FOR EVALUATION OF ROBOTIC ARM BY THE MICROSCOPE CAMERA

Three modes were proposed to measure pose accuracy (Ap) and pose repeatability (Rp). The first mode was that the gantry was stationary and only the robotic arm took the motions. The second mode was that the robotic arm was keeping the constant pose, but the gantry moved in X and Y directions. The last mode was a combined motion with the gantry and robotic arm.

In each mode, the robotic arm moved to the same point with the same pose. The commanded point should be in the field of view (FOV) of the camera, and the camera would recognize the same micro-size feature as the target (shown in Figure 9) when the robotic arm moved to the point. Meanwhile, the center of the target pixel coordinate value was acquired and recorded by the LabVIEW® program with the vision assistant function. With the calibrated resolution of the microscope camera, the actual values

of points robotic arm reaching can be measured and calculated for Ap and Rp.

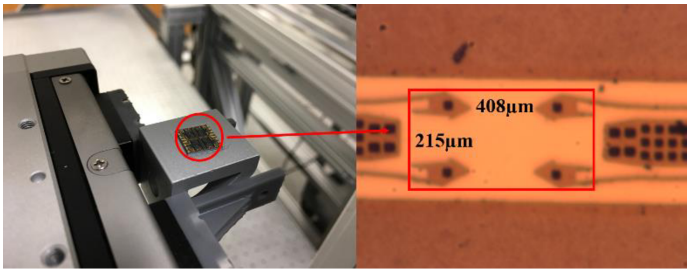

FIGURE 9: MICRON-SIZE FEATURE FOR VISUAL MEASUREMENT

For the first mode, there were 3 paths to evaluate the robotic arm performance - refer to Figure 10. The P0 was the target point, which was in the FOV of the camera, P1, P2, P3, and P4 were outside the FOV. The robotic arm performed repeatable motion between respective points.

i) 1st path: repeat linear motion between P0 and P1---X direction.
ii) 2nd path: repeat linear motion between P0 and P3---Y direction
iii) 3rd path: repeat motion along the diagonal section between P0 and P4
iv)

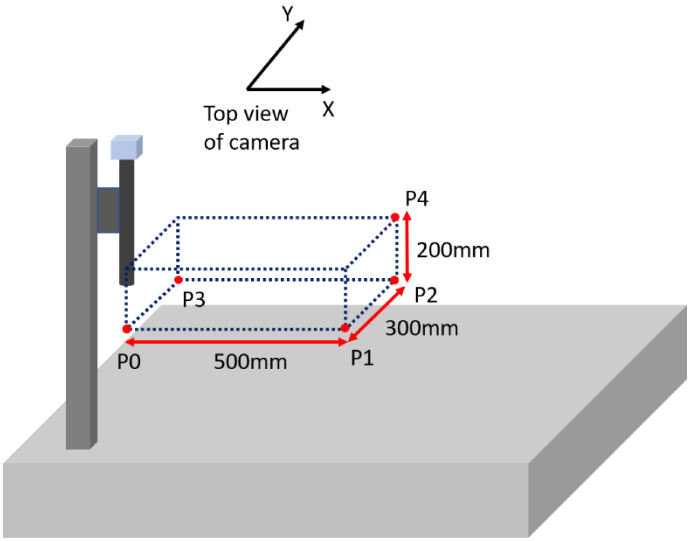

FIGURE 10: POINT LOCATIONS IN THE FIRST MODE

In the second mode, we considered motion only of the gantry along X and Y direction where the robotic arm was kept at rest in the same pose. Figure 11 shows the points that the target reached. P0' still represents the point in the FOV of the camera P1', P2', and P3' pointed outside the FOV of the camera during the gantry motion. The repeatable motion of the robotic arms was realized along the three paths.

i) 1st path: repeat the motion from P0' to P1'---X' direction.
ii) 2nd path: repeat the motion from P0' to P3'---Y' direction.
iii) 3rd path: repeat the motion from P0' to P1', P1'to P2', P2' to P3', and P3' back to P0'.

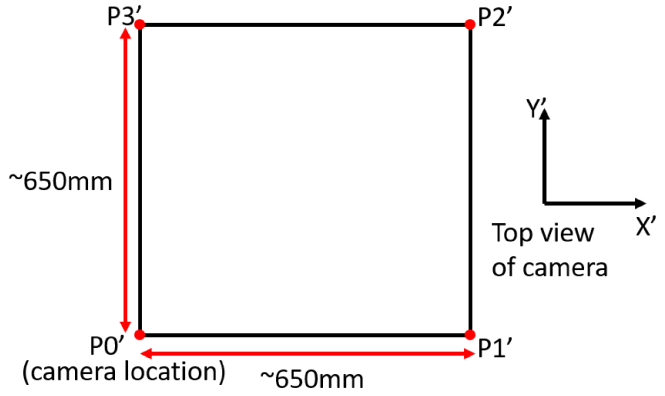

FIGURE 11: POINT LOCATIONS IN THE SECOND MODE

In the third mode, we have considered the combined motion of the gantry and robotic arm together. The sequence of the repeatable motion is described below (Figure 10 and 11):

i) The robotic arm moved from P0 to P4 along a diagonal path.
ii) Then, the gantry (with robot) moved along X-axis from P0' to P1'.
iii) Next, the gantry moved along Y-axis for the same distance between P1' and P2'.
iv) After the gantry moved back following section |P1'P2'| and |P0'P1'| to gantry's initial point at P0'.
v) Finally, the target is moved from P4 position to initial point P0.

Besides the microscope camera method, we have employed another measurement method by using two high-resolution laser displacement sensors. Figure 12 shows different arrangements of two Keyence® laser displacement sensors for measurement in X, Y, and Z directions. Keyence® instruments were used to evaluate robotic arm performance for three different modes as the same modes described in the case of the camera. The experimental results of this evaluation will be discussed in Section 4.

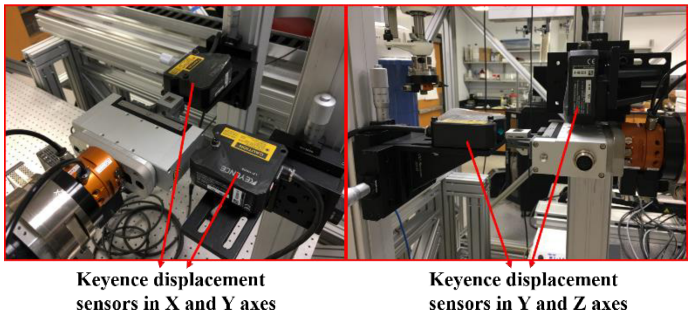

FIGURE 12: TWO LASER DISPLACEMENT SENSORS USED TO MEASURE THE POSE PERFORMANCE

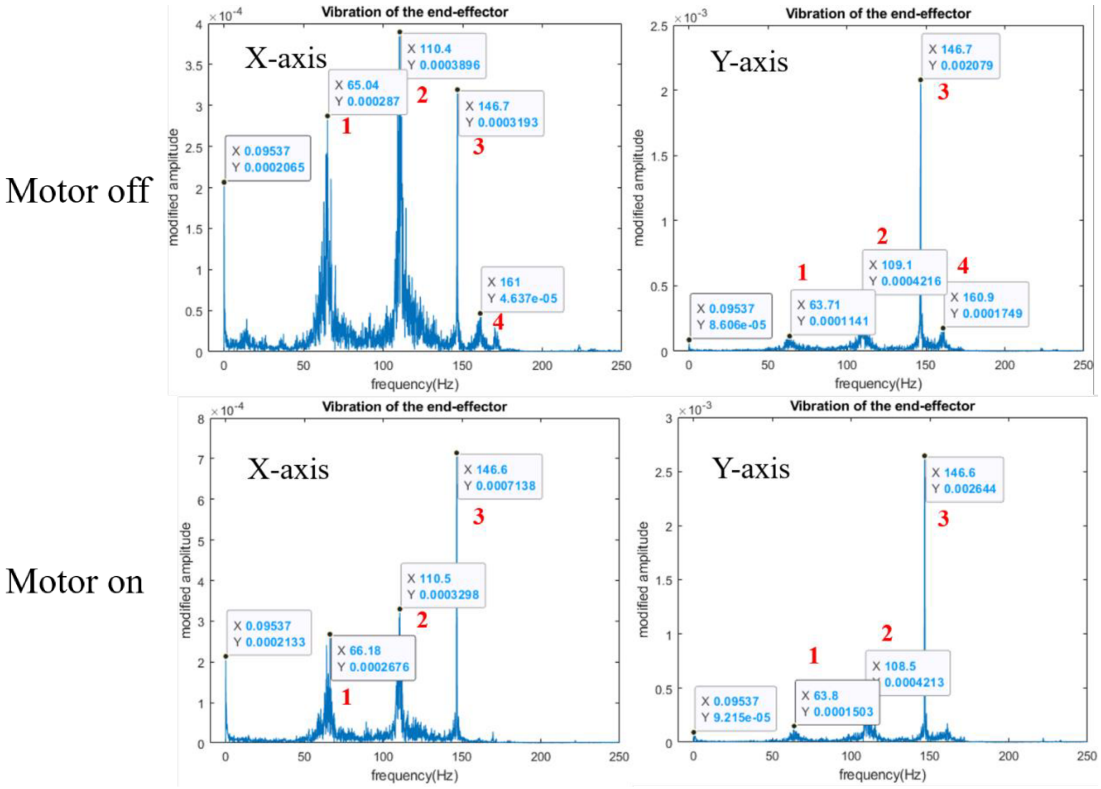

FIGURE 14: TWO LASER DISPLACEMENT SENSORS MEASURE THE NATURAL FREQUENCY OF THE ROBOTIC ARM

In the third evaluation method, we have utilized a Digimatic® indicator to evaluate the robotic arm pose performance. Due to the measurement limit of the Digimatic® indicator, it only indicated the data by touching the object, which resulted in that the Digimatic® indicator only could measure one direction of data of the robotic arm motion at once. Therefore, only one pose of the robotic arm was evaluated in the X, Y, and Z direction (shown in Figure 13).

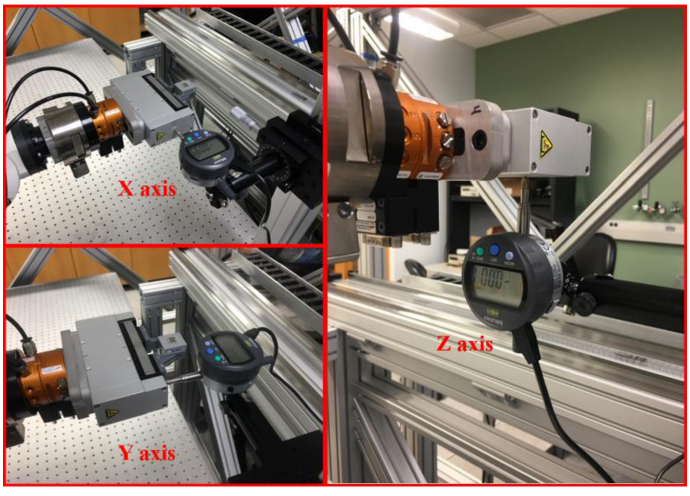

FIGURE 13: DIGIMATIC® INDICATOR USED TO MEASURE THE POSE PERFORMANCE

4. RESULTS AND DISCUSSION

First, our progressive design approach for the custom frame has significantly improved both static and dynamic responses of the structure, started from the initial design towards the final version. In Table 1, it is evident to see three eigenfrequencies begin to ramp up as a result of increased structural stiffness particularly after adding more beams at specific positions. Otherwise, the maximum deformation of the frame in each version has been successively decreased, especially in the final version, where the maximum deformation dropped from 3.5mm (in the initial version) to 0.8mm. Besides, in some modal shapes, the deformation region is shifted from the upper beams (in other version designs) into the lateral beams in the final version design which can be viewed as an additional geometrical advantage.

4.1 Vibration Performance of Frame

Prior to evaluating the pose performance of the robot, we investigated the spectral response of the positioning data collected in a static mode. The natural frequencies of vibration were estimated using the Fast Fourier Transform (FFT) algorithm dealing with the data collected by two Keyence laser displacement sensors. High peaks of frequency are shown in Figure 14 and the values are listed in Table 2. In both cases, no matter whether the robot's motor was on or off (brake off or on), the measured natural frequencies were very close for the X-axis and Y-axis, which means that the status of the motor is not a significant factor to the natural frequency of the robotic arm in

the static mode. Due to direct current offset influence, the frequency of 0.09537 Hz can be neglected in Figure 14. Moreover, the estimated simulation three eigenfrequencies of the final version of the frame's design (Table 1) are not matching any robot's structure natural frequencies determined experimentally (Figure 14). It may speculate that this frequency mismatch suggests that only the robot's motion would not induce the resonance. However, further study is needed to investigate whether the gantry motion can generate resonance in the whole frame + gantry + robotic arm structure.

TABLE 2: NATURAL FREQUENCIES (HZ) OF THE ROBOTIC ARM IN MOTOR ON AND OFF

Number	Motor off		Motor on	
	X-axis	Y-axis	X-axis	Y-axis
1	65.04	63.71	66.18	63.8
2	110.4	109.1	110.5	108.5
3	146.7	146.7	146.6	146.6
4	161	160.9	-	-

4.2 Precision metrics of the robotic arm and gantry system

After the stiffness and vibration of the frame were improved, the robotic arm was evaluated following the ISO9283:1998 standard. Two main robot performance criteria needed to be evaluated, including the robot's pose accuracy and pose repeatability. Pose accuracy represents how close the robot reaches the desired position in its workspace, and pose repeatability represents how close to the same location the robot returns repeatedly after *N* repeat cycles. Pose accuracy and pose repeatability were used in the same test conditions.

In the experiments, each path in the three different modes was repeated *N=30* times, and we collected 30 data points along with the cartesian X-axis and Y-axis, and Z-axis respectively. To estimate the accuracy and the repeatability of the robot, we used the following definitions:

$$Ap = \sqrt{(\overline{X} - X_c)^2 + (\overline{Y} - Y_c)^2 + (\overline{Z} - Z_c)^2} \quad (6)$$

$$\overline{X} = \frac{1}{N}\sum_{i=1}^{N} X_{ai} \quad (7)$$

$$\overline{Y} = \frac{1}{N}\sum_{i=1}^{N} Y_{ai} \quad (8)$$

$$\overline{Z} = \frac{1}{N}\sum_{i=1}^{N} Z_{ai} \quad (9)$$

where X_c, Y_c, and Z_c are the commanded cartesian robot positions, X_{ai}, Y_{ai}, and Z_{ai} are the attained positions, and *N* is the number of motion cycles performed. $\overline{X}$, $\overline{Y}$, and $\overline{Z}$ are the mean of attained positions. Furthermore, the pose repeatability can be calculated as:

$$Rp = \bar{l} + 3S_l \quad (10)$$

$$l_i = \sqrt{\left(X_{ai} - \overline{X}\right)^2 + (Y_{ai} - \overline{Y})^2 + (Z_{ai} - \overline{Z})^2} \quad (11)$$

$$\bar{l} = \frac{1}{N}\sum_{i=1}^{N} l_i \quad (12)$$

$$S_l = \sqrt{\sum_{i=1}^{N}(l_i - \bar{l})^2 \Big/ N - 1} \quad (13)$$

where l_i is the deviation between i-th attained positions and mean of attained positions. S_l is the standard deviation of l_i.

There are three different modes proposed to measure the pose accuracy and repeatability of the robotic arm: the motion of robot only, the motion of gantry only, and the motion combination of gantry and robot. Due to the limitation of pose measurement of the gantry, only X and Y axes motion can be measured. While the 6-DOF robotic arm can present motion in spatial space. Otherwise, there are three different types of sensors employed to measure the position values of the end-effector on the robotic arm: a microscope camera, two Keyence laser displacement sensors, and a Digimatic® indicator.

Firstly, a microscope camera was employed. Because the camera only has one DOF measurement, the microscope camera was set up in horizontal and vertical orientations to estimate the robot precision in the X, Y, and Z axes. The pose accuracy and repeatability calculated results were listed in Table 3.

In the first mode, calculated pose accuracy and repeatability of the robot along with 1st, 2nd, and 3rd paths are very similar. The probable reason for those results is that for the 1st, 2nd, and 3rd path robotic arm moves along a single and shorter section without changing the direction of the motion (only orientation in case of the repeatable motion). Nevertheless, calculated experimental repeatability is within the range of the factory value from the manufacturer +/- 30μm.

In the second mode, we analyzed only the gantry motion along with the X and Y directions. The main factors affecting precision metrics, in this case, are servo motor load, motor gearbox, gantry structure features, and payload. Different precision metrics results for the paths in the second mode are most likely caused by the structural features of the X-Y gantry and how it affects its motion. We can consider several reasons for different values of accuracy and repeatability. In Figure 11, in Y' direction (2nd path), the gantry base components were mounted on the top of the frame and rigidly supported by the structure of the frame. Whereas in X' direction (1st path), there is not much support for motion components, just rely on the stiffness of component material. That may result in different metrics between the 1st and 2nd paths. Another factor could be the payload. Analyzing gantry structure (Figure 3) in Y' direction (2nd path) servo motor with gearbox will have a smaller load since it has to move only the robotic arm with gantry adapter/fixture along 2.5m section. Whereas in the X' direction (1st path), the same servo motor with the gearbox has to move a much larger (heavier) payload. The whole 2.5m section with several long aluminum beams and the robotic arm (Figure 3). A larger payload usually results in lower accuracy and worse

repeatability. Another possible contributing factor related to the gantry's structure is the difference in motion realization for both paths. In the case of the 2nd path (Y' direction) motion is simpler where the robotic arm with adapter is transported along one linear track (Figure 3). For the 1st path (along X' direction) we consider displacement of 2.5m long structure (Figure 3) with a more complex servo motor-transmission system which might cause non-synchronous motion of both ends at the microscale.

For the 3rd path, the robot moved in a cycle path stopping at four corners which resulted in the worst result for repeatability. Here, the scenario is similar as in the case of the second mode's 1st path. As expected, repeatability is higher due to combined motion along different sections in different directions and larger travel distances. Although interestingly accuracy for the 3rd path is improved compared with the 1st and 2nd paths, it could be caused by error compensation when the robot returns to the starting point after being displaced along the square-shaped trajectory (Figure 11).

In the third mode, the combined motion of the gantry and robotic arm should be considered with various factors. 37.4μm is sort of a reasonable measurement even it is higher than 30μm due to the gantry motion factors probably as domain factors.

TABLE 3: POSE ACCURACY AND REPEATABILITY OF ROBOTIC ARM USING A MICROSCOPE CAMERA

	Accuracy (μm)	Repeatability (μm)
First mode (robot only)		
1st path	**5.3**	**8.7**
2nd path	**5.7**	**6.2**
3rd path	**5.7**	**6.2**
Second mode (gantry only)		
1st path	**40.8**	**39.3**
2nd path	**24.7**	**26.5**
3rd path	**19.7**	**39.5**
Third mode (gantry + robot)		
Combination	**9.6**	**37.4**

Also, we used two Keyence laser displacement sensors to evaluate the pose performance of the robotic arm. The motion modes are like the ones we discussed for microscope camera measurement. The pose accuracy and repeatability experimental results are listed in Table 4. The laser displacement sensor is much more precise than the microscope camera to measure objects because of the different measuring functions they have. By using the camera to measure the target position, it must utilize an image processing function to recognize the template of the target. Due to the natural vibration of the whole system, the images captured by the camera were not static but fuzzy, which results in the target position losing precision. Compared with camera measurement, laser displacement sensor is more reliable and stable based on high sampling frequency (set 50kHz), but the LabVIEW® program to collect data after image processing of the camera just has around 7.5Hz sampling frequency. Therefore, the data collected by the laser displacement sensors are reasonably resulting in the high precision of measurement.

From Table 4, the accuracy and repeatability values are almost the same in the first mode. The reason has been discussed above. But in the second mode, there is a big difference in repeatability between the 1st path and 2nd path. The reasons are probably the same as the ones discussed above for the camera measurement. The accuracy and repeatability of motion in the Y' direction are much better than in the X' direction. While the repeatability of combination motion is more than 30μm, 34.7μm also is a reasonable result after considering the repeatability of gantry and robot motion individually.

TABLE 4: POSE ACCURACY AND REPEATABILITY OF ROBOTIC ARM USING TWO LASER DISPLACEMENT SENSORS

	Accuracy (μm)	Repeatability (μm)
First mode (robot only)		
1st path	**15.6**	**11.0**
2nd path	**15.0**	**11.0**
3rd path	**10.8**	**11.8**
Second mode (gantry only)		
1st path	**10.8**	**22.7**
2nd path	**8.3**	**9.8**
Third mode (gantry + robot)		
Combination	**15.6**	**34.7**

Besides the above two methods, a Digimatic® indicator was used as another sensor to evaluate the pose accuracy and repeatability of the robotic arm. Due to its sensing principle, the Digimatic® indicator collected the data by being touched by the object. That limits the sensor to only measure one direction displacement. We only evaluated the pose accuracy and repeatability of the robot with gantry motion in X and Y axes, and the robotic arm motion in X, Y, and Z axes. The travel length of gantry motion on the X or Y axis is around 650mm while the travel length of robot motion is 500mm for X-axis, 300mm for Y-axis, and 200mm for Z-axis. There is only one direction parameter instead of three-direction parameters in the equations to calculate the pose accuracy and repeatability of single-axis motion. The calculated results are listed in Table 5.

TABLE 5: POSE ACCURACY AND REPEATABILITY OF ROBOTIC ARM USING DIGIMATIC® INDICATOR

	Accuracy (μm)	Repeatability (μm)
First mode (robot only)		
X-axis	**5.2**	**4.6**
Y-axis	**2.8**	**3.3**
Z-axis	**3.2**	**6.2**
Second mode (gantry only)		
X-axis	**22.3**	**36.2**
Y-axis	**4.0**	**9.1**

From Table 5, the repeatability in X-axis and Y-axis is almost close, but in Z-axis, the repeatability increases a little bit. That might be caused by the payload factor in Z-axis. When the robotic arm moved down to touch the indicator, Due to the inertial movement in Z-axis, it could result in the offset of displacement. Otherwise, for the gantry motion, the repeatability in X direction motion is much more than one in Y direction motion. Those results are similar to the other two sensors' experimental results. The reasons for this case should be the same.

According to the ISO standard, accuracy is a deviation between the commanded position and the measured (attained) position. Whereas repeatability is a measure of fluctuation between the measured actual positions after repeat visits to the same commanded position. Therefore, these two measures provide information about two distinct properties of the evaluated robotic system in the context of the planned tasks. There is a possible scenario where calculated accuracy can be better than repeatability.

In this case, attained positions are widely distributed due to the given experimental conditions resulting in the large value of repeatability – "bad" repeatability – in agreement with the definition (Equation 10). However, attained positions are evenly distributed (normal distribution) where the mean attained position is relatively close to the commanded position (Equation 6) resulting in a low value of accuracy – "good" accuracy.

In our study we faced an interesting situation where the pose accuracy is fluctuating relative to the pose repeatability (Tables 3 - 5) - some values are less than repeatability, but some are more than that. This is due to several factors, such as different instruments used for the position measurements, different modes, and paths during the motion of the robot/gantry system. Nevertheless, the behavior of our system reflects possible scenarios regarding the relation between accuracy and repeatability.

We would like also to pay attention to the arbitrary character of the ISO standard definition of accuracy which was discussed by other researchers [14]. Specifically, the challenge to clearly define the commanded position, which is usually associated with the robot's system of coordinate, compared to the attained position determined by the sensor, and defined in the sensor's system of coordinate.

Comparing all three types of sensors used in the experiments, we have determined that the Keyence® laser displacement sensor is more reliable and precise than the two other tools. One of the factors is the sampling rate of data acquisition. The acquisition frequency of the microscope camera drops to on 7.5Hz due to the image processing steps. For example, the LabVIEW vision assistant function was used to acquire the target coordinate information, such as pixel values at a specific location. By comparison, the Keyence® sensor sample rate can be set as high as 50KHz. Such low acquisition frequency of camera might result in low precision measurement of pose accuracy and repeatability. On the other hand, the Digimatic® indicator allows measurement only in one direction at once, thus providing less information compared to the microscope camera and the Keyence® sensors. In summary, the Keyence® laser displacement sensors allow the most reliable evaluation of the robotic arm performance in a custom robotic system.

5. CONCLUSION

A custom Aluminum frame was designed and installed to support the X-Y gantry with a ceiling-mounted 6-DOF industrial robotic arm. Given that frame's mechanical stiffness and its stability affect the robot motion performance and high precision assembly applications, a careful static and dynamic analysis of the frame was critical

Started with the initial design and considered the first 3 eigenfrequencies and total deformation as design criteria, a progressive approach to improve the initial frame design was proposed. Using the FEA technique and COMSOL® as the simulation software, we investigated and simulated 4 various modular versions of frame design aiming to increase eigenfrequency and reduce total deformation in the frame structure.

Analyzed 5 different versions, our study shows a consistent reduction occurring in maximum deflection in the frame from 3.5 mm in the initial design to 0.8mm in the final version. Similarly, considerable mitigation appeared in vibrational response, nearly by a factor of 2, as eigenfrequency jumped to 19.9Hz in the final version. In all cases, each frequency mode falls well below the measured end-effector frequency, ensuring no cross resonance will occur between the robot base (frame) and the end-effector. The nature of frame structure also allows to further increase the structural stiffness to meet special requirements and application, if necessary, in the future.

Evaluation of the robotic arm performance was realized with an Edmund microscope camera, two Keyence® displacement sensors, and a Mitutoyo Digimatic® indicator in three methods. The pose accuracy and repeatability of the robotic arm, X-Y gantry, and the combination of both were measured and calculated, respectively. Precision metrics results are consistent with expectations based on the manufacturer design metrics of the robotic arm and X-Y gantry structural features.

ACKNOWLEDGEMENTS

This work was supported by the National Science Foundation under grant MRI#1828355 and EPSCOR#1849213. We appreciate Andres Montenegro, Olalekan O. Olowo, and Douglas J. Jackson, who took the effort to assemble the frame, X-Y gantry, and robotic arm.

REFERENCES

[1] Bhatt, P. M., Kabir, A. M., Malhan, R. K., Shah, B., Shembekar, A. V., Yoon, Y. J., and Gupta, S. K., "A robotic cell for multi-resolution additive manufacturing," Proc. 2019 International Conference on Robotics and Automation (ICRA), IEEE, pp. 2800-2807.

[2] Yoon, Y. J., Yon, M., Jung, S. E., and Gupta, S. K., "Development of Three-Nozzle Extrusion System for Conformal Multi-Resolution 3D Printing With a Robotic Manipulator," Proc. International Design Engineering Technical Conferences

and Computers and Information in Engineering Conference, American Society of Mechanical Engineers, p. V001T002A024.

[3] Brethé, J.-F., Vasselin, E., Lefebvre, D., and Dakyo, B., "Determination of the repeatability of a kuka robot using the stochastic ellipsoid approach," Proc. Proceedings of the 2005 IEEE International Conference on Robotics and Automation, IEEE, pp. 4339-4344.

[4] Morozov, M., Riise, J., Summan, R., Pierce, S. G., Mineo, C., MacLeod, C. N., and Brown, R., "Assessing the accuracy of industrial robots through metrology for the enhancement of automated non-destructive testing," Proc. 2016 IEEE International Conference on Multisensor Fusion and Integration for Intelligent Systems (MFI), IEEE, pp. 335-340.

[5] Baker, J., Kurisko, T., Li, H., Poganski, D., and Worcester, J., 2014, "Development of ISO Compliant Repeatability Procedures for Evaluating Collaborative Robots," WORCESTER POLYTECHNIC INSTITUTE.

[6] Kuric, I., Tlach, V., Ságová, Z., Císar, M., and Gritsuk, I., "Measurement of industrial robot pose repeatability," Proc. MATEC Web of Conferences, EDP Sciences, p. 01015.

[7] ISO, E., 1998, "9283: 1998," Manipulating industrial robots-Performance criteria and related test methods.

[8] Wei, D., Hall, M. B., Sherehiy, A., and Popa, D. O., 2020, "Design and Evaluation of Human–Machine Interface for NEXUS: A Custom Microassembly System," Journal of Micro and Nano-Manufacturing, 8(4).

[9] Wei, D., Hall, M. B., Sherehiy, A., Kumar Das, S., and Popa, D. O., "Design and Evaluation of Human-Machine Interface for NEXUS: A Custom Microassembly System," Proc. ASME 2020 15th International Manufacturing Science and Engineering ConferenceV002T08A018.

[10] McGrady, G., and Walsh, K., "Dual Extrusion FDM Printer for Flexible and Rigid Polymers," Proc. International Manufacturing Science and Engineering Conference, American Society of Mechanical Engineers, p. V001T001A009.

[11] McGrady, G., and Walsh, K., "Embedding Sensing Capabilities in FDM-Printed Objects."

[12] Tofangchi, A., Han, P., Izquierdo, J., Iyengar, A., and Hsu, K., 2019, "Effect of Ultrasonic Vibration on Interlayer Adhesion in Fused Filament Fabrication 3D Printed ABS," Polymers, 11(2), p. 315.

[13] Deshpande, A., and Hsu, K., 2018, "Acoustoplastic metal direct-write: towards solid aluminum 3D printing in ambient conditions," Additive Manufacturing, 19, pp. 73-80.

[14] Liu, H., 2015, "Environment for Industrial RobotPerformance Evaluation."